Journal of Analytical Sciences, Methods and Instrumentation, 2018, 8, 49-64
http://www.scirp.org/journal/jasmi
ISSN Online: 2164-2753
ISSN Print: 2164-2745

Experimental Investigation of Effects of Electric Operating Parameters on Pulsed Corona Discharges in Humid Air at Atmospheric Pressure

Hasna Guedah[1], Alyen Abahazem[1,2*], Nofel Merbahi[3], Mohamed Yousfi[3], Karim Saber[1], Ahmed Ihlal[1]

[1]Laboratory Materials and Renewable Energies, Physics Department, Ibn Zohr University, Agadir, Morocco
[2]CRMEF-SM, Inezgane, Morocco
[3]LAPLACE UMR 5213-CNRS, Paul Sabatier University, Toulouse, France
Email: *a.abahazem@uiz.ac.ma

How to cite this paper: Guedah, H., Abahazem, A., Merbahi, N., Yousfi, M., Saber, K. and Ihlal, A. (2018) Experimental Investigation of Effects of Electric Operating Parameters on Pulsed Corona Discharges in Humid Air at Atmospheric Pressure. *Journal of Analytical Sciences, Methods and Instrumentation*, **8**, 49-64.
https://doi.org/10.4236/jasmi.2018.84005

Received: November 12, 2018
Accepted: December 22, 2018
Published: December 25, 2018

Abstract

The present work is devoted to electrical and optical study of a point-plane atmospheric pressure corona discharge reactor in humid air powered by pulsed high voltage supply. The corona current and the injected energy are analyzed as a function of several parameters such as applied voltage and humidity rate. Then, investigations based on emission spectroscopy analysis were used in UV range (from 200 nm to about 400 nm). The main observed excited species were the second positive (SPS), the first negative (FNS) systems and OH(A-X) rotational bands. The latter band was used to simulate the rotational temperature (T_r), whereas the N_2^+ (FNS) band was used to determine the vibrational temperature (T_v). The electron temperature (T_e) is determined from the ratio of line intensities of the spectral bands of both N_2^+ FNS at 391.4 nm and N_2SPS at 394.4 nm. The rotational, vibrational and electronic temperatures are analyzed as a function of above parameters (applied voltage, frequency and hygrometry rate) near the anodic tip. As well we study the axial variation of electronic temperature for a fixed applied voltage at 6.4 kV, frequency at 10 kHz and 100% of humidity. It is found that the rotational, vibrational and electronic temperatures increased with increasing applied voltage, frequency and humidity rate. The increase of rate hygrometry for an inter-electrode distance fixed at 10 mm causes an increase in both the amplitude of the corona current discharge and the energy injected in corona discharge. This is indicative of more intense reactive plasma while increasing hygrometry rate.

Keywords

Corona Discharge, Atmospheric Pressure, Optical Emission Spectroscopy, Pulsed High Voltage, Humidity

1. Introduction

Non-thermal plasmas at atmospheric pressure are very efficient sources of active species (radicals, excited species, charged particles, UV radiations, etc.). Many applications can be fulfilled from such non-thermal plasmas, for example in the environmental domain (gas pollution control [1] [2] [3]) or in the fields of biology and medicine [4]-[9] or in many other applications (surface treatment [10] [11] [12], plasma actuators [13], etc.). In fact, the optimization of the active species in these non-thermal plasmas produced by corona discharges under pulsed voltage in humid air needs to be adapted and optimized in a very specific way for each targeted application. In the case of corona discharges, there are two stages during streamer discharge evolution, the primary streamer [14] [15] and the secondary one [16]. The primary streamer is an instantaneous propagation of a strong ionization region (during about 50 ns or shorter), and the secondary streamer appears after the primary streamer arrival at the cathode [17]. The positive corona characteristics can be affected by many factors, such as the applied voltage, electrode configuration, and background gas composition [18] [19] [20] [21]. During the last two decades it has been reported that humidity has some impact on the behavior of atmospheric corona discharges [22] [23]. Our work includes two parts, in the first part we study, the influence of some operating parameters (applied voltage and humidity) on the corona current and the energy injected in corona. The second part is dedicated to spectroscopic studies of some molecular spectra emitted in the UV range and corresponding to N_2(SPS), N_2^+ (FNS) and OH(A-X) have been identified, located in the near-UV region. Under some very specific conditions, the measured intensity ratio of N_2^+ (FNS) over N_2(SPS) lines is known to depend on electron energy in the discharge [24]. The rotational and vibrational temperatures of the main particles (*i.e.*, excited N_2, N_2^+ ions and OH radicals) are derived from comparisons of experimental and synthetic spectra by using literature spectral simulation softwares (Lifbase [25] and Specair [26]). The knowledge of T_r, T_v, and T_e temperatures is useful in plasma processes. Indeed, electronic temperature (T_e) determines the degree of ionization of plasma. Vibrational temperature (T_v) controls the population density of the vibrationally excited molecular bands. These excited molecules play a key role in enhancing the reactivity of the plasma. The rotational temperature (T_r) of molecular species is an indicator of neutral gas kinetic temperature T_g, in atmospheric pressure low temperature plasmas.

The main objective of this paper is to emphasis the influence of the applied voltage and the hygrometry rate on corona current and injected energy, then we

will discuss the influence of various operating parameters, such as, the magnitude of high voltage, frequency and hygrometry rate, on T_r, T_v and T_e, in the objective to understand better the influence of our parameters on the behavior of the corona discharge obtained in humid air.

2. Experimental Setup

Figure 1 shows a schematic diagram of experimental setup already described in previous work [27]. Briefly, positive corona discharges are ignited under a positive pulsed high voltage, by using point to plane arrangement in a closed cell made of stainless steel at atmospheric pressure. The point of tungsten is machined starting from a stem of 1 mm of diameter and 5 mm of length and its final tip radius ρ, is around 25 µm. The plane electrode is a disc of copper with 4 cm diameter and 2 cm thickness. The inter-electrode distance, d, can be easily adjustable from the outside by means of a Z column, without opening the reactor.

The humid air was generated by Controlled Evaporation Mixing system (CEM) Bronkhorst. This CEM-system consists of three parts:

- Mass Flow Controller for Gas: Control and measurement and control of the carrier gas flow,
- Mass Flow controller for Liquids: Control and measurement of the liquid flow,
- Mixing Valve and Evaporator: for control of the liquid source flow and mixing the liquid with the carrier gas resulting in total evaporation.

During our experiments, the humid air was obtained by fixing the air flow and the water flow.

The discharge is generated by using a pulsed high-voltage supply by a TTL

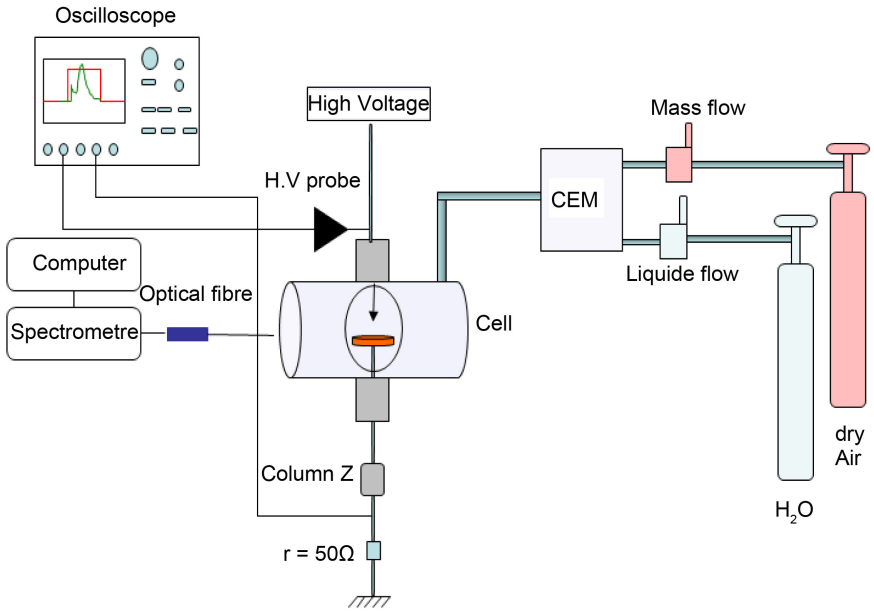

Figure 1. Schematic diagram of the experimental device.

which can adjust the frequency and the pulse width of the applied voltage. The gap voltage $U_g(t)$ is measured using a high voltage probe (PPE 20 kV) and the instantaneous discharge current $i(t)$ is obtained through 50 Ω resistance. The relevant voltages are recorded using a 5 GHz digital sampling 500 MHz oscilloscope. Typical waveforms of measured voltage and current are shown in Figure 2.

Optical fiber is used for collecting light emission from the discharge chamber. The delivered light is split by a monochromator in which is dispersed by a diffraction grating and detected by a CCD sensor. The monochromator has a focal length of 0.75 m (2700i SpectraPro Acton Research Corporation) and equipped with a set of three diffraction gratings (600, 1800 and 2400 grooves mm^{-1}) to analyze the emitted light from the discharge. It has an output port with an ICCD camera (PI-MAX, Princeton Instruments) for continuously spectral measurements. Spectral scanning is achieved with a computer-controller.

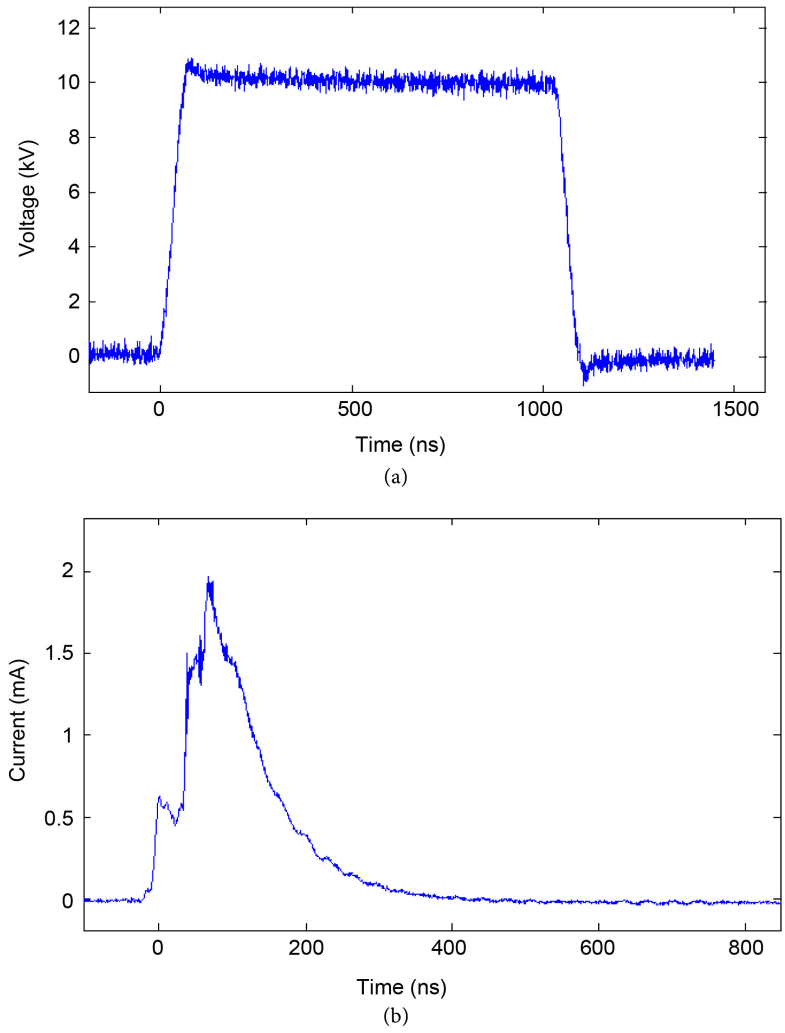

Figure 2. Waveform of voltage (a) and current (b) in humid air at atmospheric pressure for: V_a = 9 kV, d = 10 mm, ρ = 25 μm, f = 1 kHz, τ = 1 μs and hygrometry rate: 100%.

3. Results and Discussions

3.1. Electrical Analysis of Pulsed Corona Discharges in Humid Air at Atmospheric Pressure

3.1.1. Influence of Applied Voltage

Figure 3 shows the corona current discharge for several applied voltages in air with 100% of water vapor at atmospheric pressure for a gap distance of 10 mm, a frequency of 1 kHz and a pulse width of 1 µs. In the case of 9 kV, the streamer starts near the point corresponding to the higher electric field region favoring the electron multiplication. Its propagation towards the cathode plane develops a conductive channel which overlay the whole gap. This propagation of the cathode directed streamer is associated to the first current increase observed in the first 30 ns in Figure 2. This propagation phase include a steep increase of the corona current up to the first pick (from 25 to 27 ns) corresponds to the arrival streamer at the cathode. Secondary avalanche develops from the anode and this explains the second pick observed in Figure 3. During the extinction phase, a current relaxation is observed up to the next current pulse.

The variation of the discharge current shows that the increase in the applied voltage for an inter-electrode distance fixed at 10 mm causes an increase of the corona current amplitude. Figure 4 shows the variation of the injected energy in corona discharge as a function of applied voltages in air with 100% of water vapor at atmospheric pressure. The energy injected in corona discharge increase with the increase of applied voltage for a fixed humidity rate at 100% and gap electrode of 10 mm.

These observations are due to the spatial variation of applied geometric field as a function of applied voltage. In fact, the high geometric electric field conducts

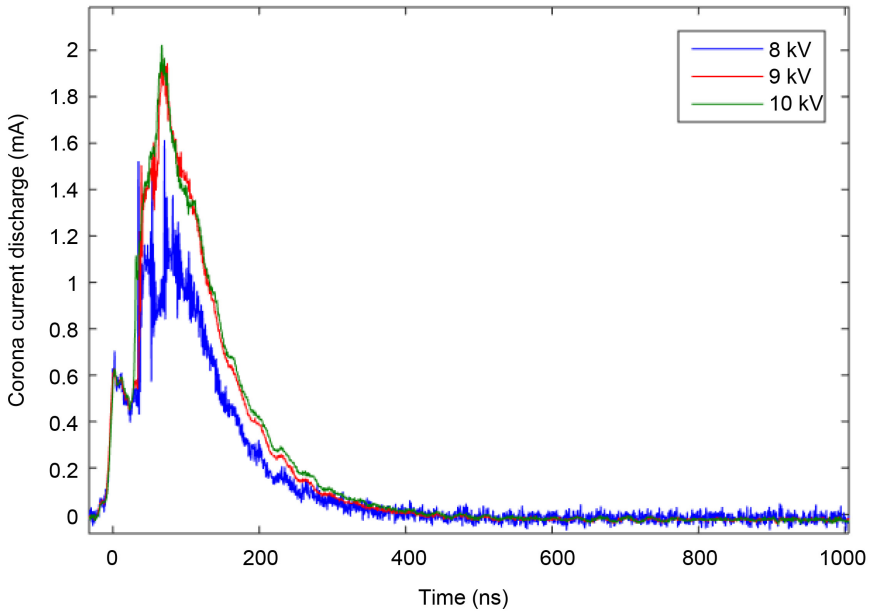

Figure 3. Discharge current in humid air at atmospheric pressure for different applied voltage, $d = 10$ mm, $\rho = 25$ µm, $f = 1$ kHz, $\tau = 1$ µs and humidity rate: 100%.

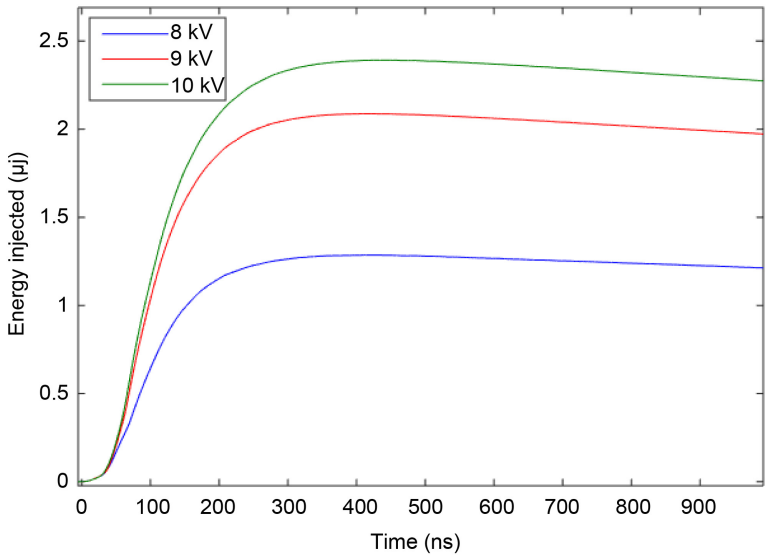

Figure 4. Energy injected in corona discharge in humid air at atmospheric pressure for different applied voltages, $d = 10$ mm, $\rho = 25$ µm, $f = 1$ kHz, $\tau = 1$ µs and hygrometry rate: 100%.

to a strong amplification of the electronic avalanche by the energetic electrons. A similar variation was observed in the case of corona discharge in dry air at atmospheric pressure [28].

3.1.2. Influence of Hygrometry Rate

Figure 5 and **Figure 6** give the variation of respectively the corona current discharge and the injected energy for two hygrometry rates at atmospheric pressure for a gap distance of 10 mm, a frequency of 1 kHz and a pulse width of 1 µs. The variation of the discharge current shows that the increase in the hygrometry rate causes an increase in the amplitude of corona current discharge leading to the increase of the injected energy. This is explained by growing the quantities of water vapor. In fact, the gas becomes electronegative and contributes to increase the ionization efficiency of electrons.

3.2. Optical Study of Pulsed Corona Discharges in Humid Air at Atmospheric Pressure

The emission spectra were further analyzed to find out electron temperature (T_e), vibrational temperature (T_v) and rotational temperature (T_r) [29] [30]. Electron temperature determines the degree of ionization of plasma and the primary chemical reactions; the rotational excitation is used as a global thermometer since it is generally representative of the gas temperature, whereas the vibrational excitation due to its adiabatic character can trap energy and plays the role of energy tank, which is important for chemical reactions in plasmas since it contributes to generate important secondary chemical reactions [24].

The spectroscopic study of corona discharge, in the wavelength domain from 200 nm up to about 400 nm, presented in this work, concerns mainly the variation

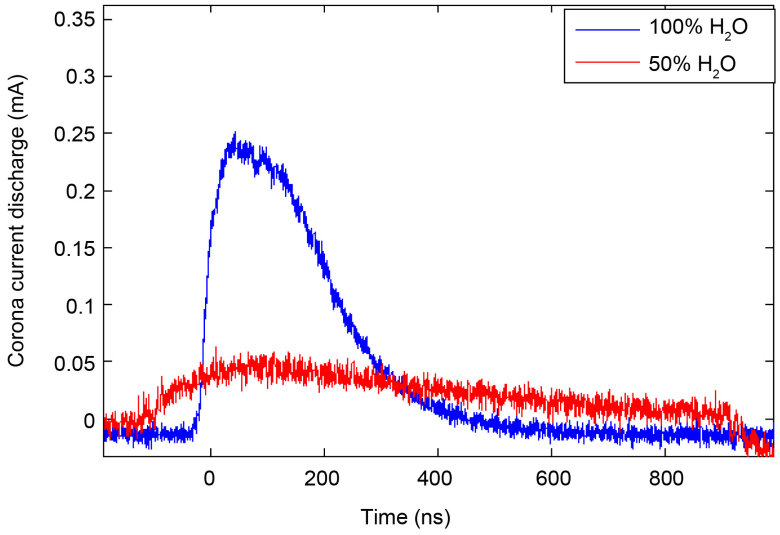

Figure 5. Discharge current in humid air at atmospheric pressure for two hygrometry rates, $d = 10$ mm, $\rho = 25$ µm, $V_a = 6.4$ kV, $f = 10$ kHz, $\tau = 1$ µs.

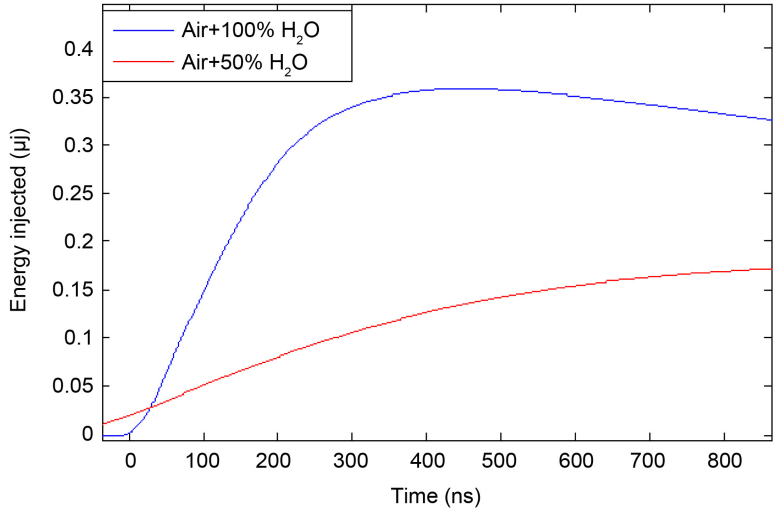

Figure 6. Injected energy in corona discharge in humid air at atmospheric pressure for two hygrometry rate, $d = 10$ mm, $\rho = 25$ µm, $V_a = 6.4$ kV, $f = 10$ kHz, $\tau = 1$ µs.

of the pulsed applied voltage, frequency and hygrometry rate to understand the influence of our parameters on the behavior of the corona discharge obtained in humid air near the anodic tip ($z = 0$). The objective is to analyze their influences on the vibrational, rotational and electronic temperatures. Then the axial variation of electronic temperature will complete the spectroscopic study to visualize the development of the discharge in the inter-electrode space [29].

3.2.1. Rotational Temperature

In humid air plasmas, the emission of OH(A-X) rotational bands between 306 nm and 310 nm provides a particularly convenient way to measure the rotational temperature. The OH(A-X) rotational bands are one of most intense systems

emitted by low temperature air plasmas sources containing H_2 or H_2O [31] [32]. In our conditions, the variation of operating parameters (voltage, frequency and hygrometry) leads to qualitatively equivalent emission spectra of OH(A-X) with a change on only the spectra intensity. Figure 7 displays the measured emission of OH(A-X) rotational bands for the same exposure time (t_{expo} = 120 s), diffraction grating (2400 grooves/mm) and diameter of the optical fiber (1 mm).

The rotational temperature was obtained by fitting the experimental spectrum with the simulated one on the entire band of OH(A-X), or more simply from the relative intensities of two groups of rotational lines corresponding to the R and Q branches of the OH(A-X) (0, 0) rotational branch at about 307 nm and 309 nm, respectively (see Figure 7). Indeed, this technique provides a sensitive thermometer since the relative intensity of the two peaks varies more or less with the rotational temperature. The effect of operating parameters on the rotational temperature is summarized in Table 1.

There is practically no rotational temperature variation as a function of the operating parameters (applied voltage, frequency and hygrometry rate), of about 300 K. It is suggested that this rotational temperature of OH is in equilibrium with the gas temperature. The assumption that the gas temperature is equal to the rotational temperature is only valid when the rotational population distribution

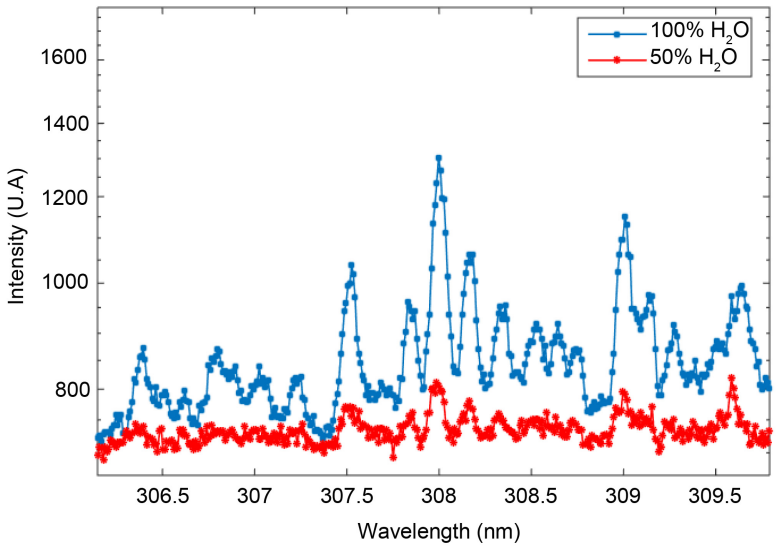

Figure 7. R and Q branches of OH(A-X) (0, 0) band system at 307 nm and 309 nm, respectively emitted near the tip in humid air at atmospheric pressure for different RH, d = 10 mm, τ = 1 µs, ρ = 25 µm, V_a = 6.4 kV and f = 10 kHz.

Table 1. Effect of operating parameters on the rotational temperature.

	Effect of applied voltage		Effect of frequency		Effect of hygrometry rate	
	V_a = 6 kV, f = 10 kHz, RH = 100%	V_a = 6.4 kV, f = 10 kHz, RH = 100%	f = 5 kHz, V_a = 6.4 kV, RH = 100%	f = 10 kHz, V_a = 6.4 kV, RH = 100%	RH = 50%, f = 10 kHz, V_a = 6.4 kV	RH = 100%, f = 10 kHz, V_a = 6.4 kV
T_r(K)	300	300	300	300	300	300

is in equilibrium with the translational temperature of the heavy species and thus thermalization of the rotational population distribution by collisions with the heavy species has occurred. Due to the highly collisional nature of atmospheric pressure plasmas this is often considered as a good assumption [33].

3.2.2. Vibrational Temperature

The vibrational temperature T_v was determined from the N_2^+ (FNS) spectra using the intensity ratio of the two head bands of N_2^+ (FNS: 1, 1) at 388.4 nm and N_2^+ (FNS: 0, 0) at 391.4 nm (see **Figure 8**). In fact, this ratio depends on the couple $\{T_r, T_v\}$ and in our case we assumed that T_r is already given by OH(A-X) spectra. Then, T_v can be estimated from the comparison of the measured intensity ratio with the calculated ones using LIF Base software. The best fit is obtained for a couple of T_r and T_v that are displayed in **Table 2** versus the operating parameters (applied voltage, frequency and hygrometry rate).

Table 2 shows that the vibrational temperature decreases with the increase of applied voltage and hygrometry rate and also increase with frequency. This T_v variation is probably due to the variation of vibration-vibration collision frequency

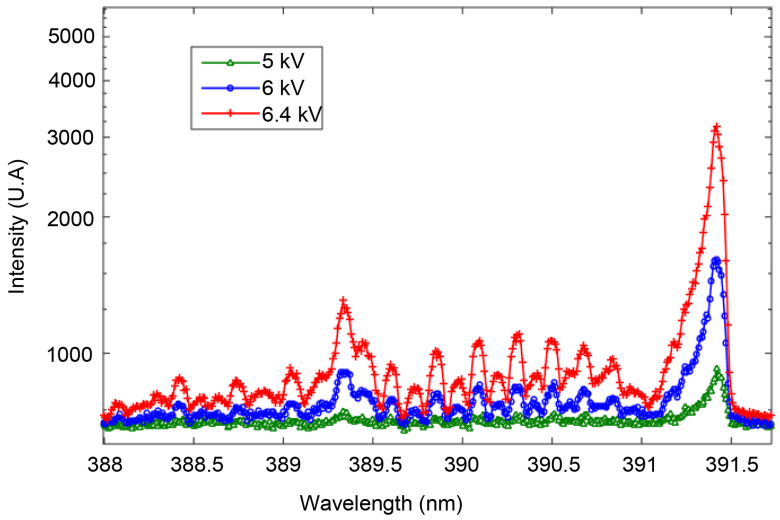

Figure 8. N_2^+ (FNS: 1, 1) and N_2^+ (FNS: 0, 0) spectra with head band at respectively 388.4 nm and 391.4 nm emitted near the tip in humid air at atmospheric pressure for different applied voltages, d = 10 mm, τ = 1 µs, ρ = 25 µm, f = 10 kHz and RH =100%.

Table 2. Effect of operating parameters on the vibrational temperature.

	Effect of applied voltage		Effect of frequency		Effect of hygrometry rate	
	V_a = 6 kV, f = 10 kHz, RH = 100%	V_a = 6.4 kV, f = 10 kHz, RH = 100%	f = 5 kHz, V_a = 6.4 kV, RH = 100%	f = 10 kHz, V_a = 6.4 kV, RH = 100%	RH = 50%, f = 10 kHz, V_a = 6.4 kV	RH = 100%, f = 10 kHz, V_a = 6.4 kV
T_r(K)	300	300	300	300	300	300
T_v(K)	1840	1820	1700	1820	1980	1820

that producing high vibration levels when the operating parameters were changed.

3.2.3. Electronic Temperature

The energy of electrons in a streamer discharge is an essential parameter that directly influences the quantity and type of dissociated species, radicals and ions. More particularly the species formed during primary collisions between energetic free electrons and molecules of background gas. This is why electron energy is among the most fundamental parameters in gas plasma discharges and is among the most fundamental parameters in gas plasma discharges and plays a very important role in understanding the discharge physics and optimization of the operation of plasma.

In the case of discharge, if the relative intensity of second positive system $N_2\left(C^3\pi_u\right)$ and first negative system $N_2^+\left(B^2\Sigma_u^+\right)$ is changed, it means that there is a variation of the average electron energy and electron energy distribution function (EEDF) that reflects more particularly a change on the energy needed for the ionization of upper level of FNS ion nitrogen molecule (18.7 eV) and also the excitation of upper level of SPS excited nitrogen molecule (11 eV) [34] [35].

Figure 9 shows N_2(SPS: 2, 5) and N_2^+ (FNS: 0, 0) spectra with head band at respectively 394.3 nm and 391.4 nm emitted near the tip of the corona discharge in humid air at atmospheric pressure. When the operating parameters (applied voltage, frequency and hygrometry rate) are changed, we observed a change of the relative intensity of emission spectra. These results mean a change in the ratio $I_{N_2^+}/I_{N_2}$ and therefore in the average electron energy.

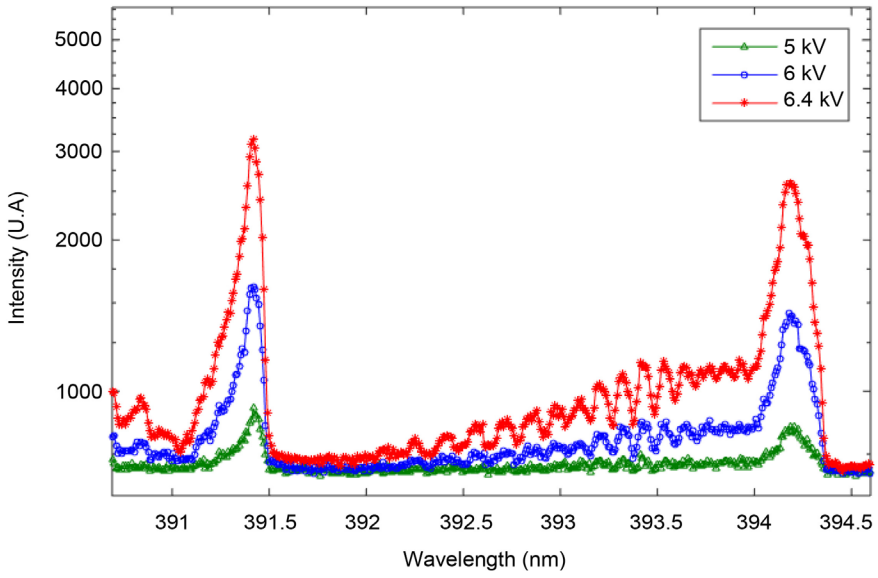

Figure 9. N_2(SPS: 2, 5) and N_2^+ (FNS: 0, 0) spectra with head band at respectively 394.3 nm and 391.4 nm emitted near the tip in humid air at atmospheric pressure for different applied voltages, d = 10 mm, τ = 1 µs, ρ = 25 µm, f = 10 kHz and RH = 100%.

We used an OES approach based on relation between the ratio $I_{N_2^+}/I_{N_2}$ of these measured head band intensities spectra and the electron temperature T_e. In fact, there are in the literature similar methods to obtain electron temperature from optical emission spectra (OES) [36] [37]. In the present work, the method developed by Zerrouki *et al.* was used. This method is based on the experimental ratio $I_{N_2^+}/I_{N_2}$ of the closest first negative system of nitrogen peaking at 391.4 nm and the second positive system peaking at 394.3 nm [37]. Zerrouki *et al.* assumed that T_e can be estimated from solution of the following equation coming from the balance of creations and losses of the excited upper level participating to the emission of N_2(SPS: 2, 5) and N_2^+ (FNS: 0, 0) transitions:

$$\frac{K_1(T_e)}{\nu_{rad1}+K_{Q1-N_2}[N_2]+K_{Q1-O_2}[O_2]} = \frac{I_{SPS}}{I_{FNS}}\times Cst\times\frac{K_2(T_e)}{\nu_{rad2}+K_{Q2-N_2}[N_2]+K_{Q2-O_2}[O_2]} \quad (1)$$

where the different coefficients are already defined and given in reference [37]. Shortly, Cst is a constant $Cst\approx\frac{A_{FNS}}{A_{SPS}}\times\frac{\lambda_{SPS}}{\lambda_{FNS}}$ and $K_1(T_e)$, K_{Q1-N_2}, K_{Q1-O_2}, ν_{rad1} are rates of creations and losses of the upper level of N_2(SPS) emission while $K_2(T_e)$, K_{Q2-N_2}, K_{Q2-O_2}, ν_{rad2} are rates of creations and losses of the upper level of N_2^+ (FNS) emission.

Knowing the experimental ratio $\frac{I_{SPS}}{I_{FNS}}$, T_e can be estimated when the equality between left and right hand sides of Equation (1) is verified during the variation of T_e.

Data for electron reaction coefficients $K_1(T_e)$ and $K_2(T_e)$ are calculated versus T_e from multi-term solution of Boltzmann equation [38] for the electron energy distribution function (EEDF). This enables us to avoid the classical overestimations of electron rate coefficients due to the classical use of Maxwell distribution. Then, the set of electron-N_2 collisions cross sections are taken from [39]. Using data of the intensity ratio $R_{394/391}$, electron mean energy is obtained from the crossing of the two curves corresponding respectively to left and right hand terms of Equation (1) (see **Figure 10**).

The electron temperature using the present method based on emission intensity ratio $R_{394/391}$ is summarized in **Table 3** for different operating parameters (applied voltage, frequency and hygrometry rate) and in **Table 4** for different positions along the discharge axis from the anode tip (z = 0 mm) to the cathode plane (z = 10 mm). First of all, the variation of the electron temperature versus the operating parameters remains because the ratio $\frac{I_{SPS}}{I_{FNS}}$ does not significantly versus these different parameters whether for instance the voltage, the frequency or the position along the inter-electrode gap.

For instance, in the case of **Table 3**, electron temperature increase with the increase of applied voltage for a rate hygrometry fixed at 100% and the frequency

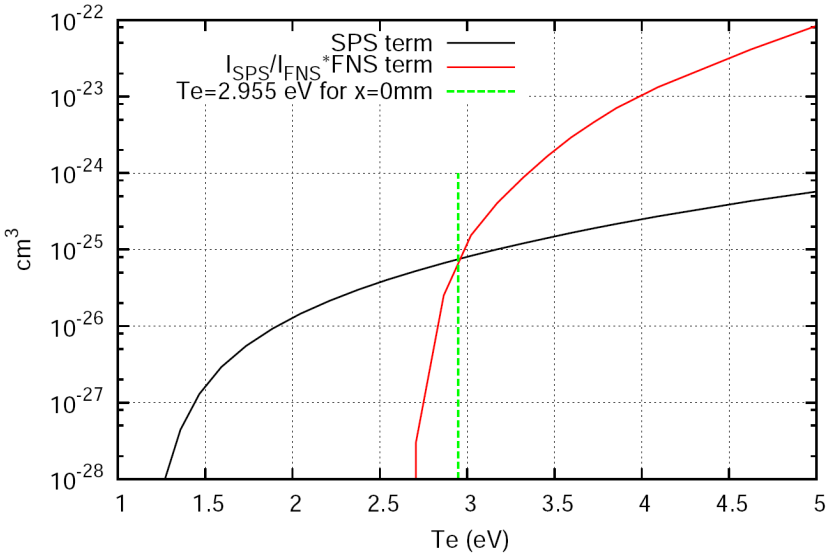

Figure 10. Left hand term and right hand term of Equation (1) and the crossing point between the two curves giving an electron temperature $T_e = 2.955$ eV for $x = 0$ mm, $V_a = 6.4$ kV, $f = 10$ kHz and $RH = 100\%$.

Table 3. Effect of operating parameters on the electronic temperature.

	Effect of applied voltage		Effect of frequency		Effect of hygrometry rate	
	$V_a = 6$ kV, $f = 10$ kHz, $RH = 100\%$	$V_a = 6.4$ kV, $f = 10$ kHz, $RH = 100\%$	$f = 5$ kHz, $V_a = 6.4$ kV, $RH = 100\%$	$f = 10$ kHz, $V_a = 6.4$ kV, $RH = 100\%$	$RH = 50\%$, $f = 10$ kHz, $V_a = 6.4$ kV	$RH = 100\%$, $f = 10$ kHz, $V_a = 6.4$ kV
T_e(eV)	2.960	2.970	2.957	2.970	2.961	2.970

Table 4. Electron temperature versus axial inter-electrode position for $V_a = 6.4$ kV, $f = 10$ kHz and $RH = 100\%$.

z(mm)	$z = 0$	$z = 2$	$z = 4$	$z = 5$	$z = 6$	$z = 8$	$z = 10$
T_e(eV)	2.955	2.964	2.955	2.954	2.953	2.951	2.949

of 10 kHz. The reasons of the small increasing electron temperature observed in Table 3 are due to the fact that with increasing voltage, the ionization efficiency of electrons increase, the free electrons are collecting more energy from the increased electric field. Same effect observed for rate hygrometry and frequency; the increase in the hygrometry rate and frequency causes a small increase in the electron temperature. This effect can be explained by the fact of increasing the quantities of water vapor that contributes to increase the ionization efficiency of electrons.

In the case of Table 4, T_e does not also vary significantly and remains close to about 2.95 eV whatever the inter-electrode position because we are in presence of corona discharge developing streamer branching structure and not a mono-filament like in DC or quasi DC case where a truly decreasing variation of electron temperature can be observed [37].

4. Conclusions

The electrical and optical studies of a point-to-plane atmospheric pressure corona discharge reactor in humid air powered by pulsed high voltage supply have been performed.

In electrical studies, the corona current discharge and the energy injected are analyzed as a function of several parameters (applied voltage and hygrometry rate). As results, the increase of rate hygrometry for an inter-electrode distance fixed at 10 mm causes an increase in both the amplitude of the corona current discharge and the energy injected in corona discharge. This is indicative of more intense reactive plasma while increasing hygrometry rate.

The optical study, in the wavelength domain from 200 nm up to about 400 nm, has been employed to determine electron temperature (T_e), vibrational temperature (T_v) and rotational temperature (T_r). These temperatures are analyzed as a function of applied voltage, frequency and hygrometry rate, near the anodic tip ($z = 0$). It is found that the rotational temperature does not change with the variation of the operating parameters (applied voltage, frequency and hygrometry rate); it remains close to about 300 K. In addition, the vibrational temperature decreases with the increase of applied voltage and hygrometry rate and also increases with frequency. The electronic temperature increases with the increase of applied voltage, hygrometry rate and frequency.

Then the axial variation of electronic temperature for a fixed applied voltage at 6.4 kV, frequency at 10 kHz and 100% of humidity is studied to visualize the development of the discharge in the inter-electrode space. This result shows no significant change and remains close to about 2.95 eV whatever the inter-electrode position because we are in presence of corona discharge developing streamer branching structure and not a mono-filament like in DC or quasi DC case where a truly decreasing variation of electron temperature can be observed.

Conflicts of Interest

The authors declare no conflicts of interest regarding the publication of this paper.

References

[1] Penetrante, B.M. and Schultheis, S.E. (1993) Non Thermal Plasma Techniques for Pollution Control, Part A&B. Springer-Verlag, Berlin, Heidelberg. https://doi.org/10.1007/978-3-642-78476-7

[2] Eichwald, O., Yousfi, M., Hennad, A. and Benabdessadok, M.D. (1997) Coupling of Chemical Kinetics, Gas Dynamics, and Charged Particle Kinetics Models for the Analysis of NO Reduction from Flue Gases. *Journal of Applied Physics*, **82**, 4781-4794. https://doi.org/10.1063/1.366336

[3] Kim, H.-H. (2004) Nonthermal Plasma Processing for Air-Pollution Control: A Historical Review, Current Issues, and Future Prospects. *Plasma Processes and Polymers*, **2**, 91-110. https://doi.org/10.1002/ppap.200400028

[4] Laroussi, M. (2002) Nonthermal Decontamination of Biological Media by Atmos-

pheric-Pressure Plasmas: Review, Analysis, and Prospects. *IEEE Transactions on Plasma Science*, **30**, 1409-1415. https://doi.org/10.1109/TPS.2002.804220

[5] Pointu, A.M., Ricard, A., Dodet, B., Odic, E., Larbre, J. and Ganciu, M. (2005) Production of Active Species in N2-O2 Flowing Post-Discharges at Atmospheric Pressure for Sterilization. *Journal of Physics D*: *Applied Physics*, **38**, 1905-1909. https://doi.org/10.1088/0022-3727/38/12/009

[6] Fridman, G., Friedman, G., Gutsol, A., Shekhter, A.B., Vasilets, V.N. and Fridman, A. (2008) Applied Plasma Medicine. *Plasma Processes and Polymers*, **5**, 503-533. https://doi.org/10.1002/ppap.200700154

[7] Stoffels, E., Roks, A.J.M. and Deelman, L.E. (2008) Delayed Effects of Cold Atmospheric Plasma on Vascular Cells. *Plasma Processes and Polymers*, **5**, 599-605. https://doi.org/10.1002/ppap.200800028

[8] Moshkunov, S.I., Khomich, V.Y. and Shershunova, E.A. (2018) A Compact Source of Flash-Corona Discharge for Biomedical Applications. *Technical Physics Letters*, **44**, 84-86. https://doi.org/10.1134/S1063785018010157

[9] Sivachandiran, L. and Khacef, A. (2017) Enhanced Seed Germination and Plant Growth by Atmospheric Pressure Cold Air Plasma: Combined Effect of Seed and Water Treatment. *RSC Advances*, Royal Society of Chemistry, **7**, 1822-1832. https://doi.org/10.1039/C6RA24762H

[10] Kunhardt, E.E. (2000) Generation of Large-Volume, Atmospheric-Pressure, Nonequilibrium Plasmas. *IEEE Transactions on Plasma Science*, **28**, 189-200. https://doi.org/10.1109/27.842901

[11] Fang, Z., Qiu, Y. and Kuffel, E. (2004) Formation of Hydrophobic Coating on Glass Surface Using Atmospheric Pressure Non-Thermal Plasma in Ambient Air. *Journal of Physics D Applied Physics*, **37**, 2261-2266. https://doi.org/10.1088/0022-3727/37/16/007

[12] Bhoj, A.N. and Kushner, M.J. (2008) Repetitively Pulsed Atmospheric Pressure Discharge Treatment of Rough Polymer Surfaces: I. Humid Air Discharges. *Plasma Sources Science and Technology*, **17**, Article ID: 035024. https://doi.org/10.1088/0963-0252/17/3/035024

[13] Eichwald, O., Bayle, P., Yousfi, Y. and Jugroot, M. (1998) Modeling and Three Dimensional Simulation of the Neutral Dynamics in an Air Discharge Confined in a Microcavity. II. Analysis of the Wall and Geometry Effects. *Journal of Applied Physics*, **84**, 4716-4726. https://doi.org/10.1063/1.368714

[14] Mraihi, A., Merbahi, N., Yousfi, M., Abahazem, A. and Eichwald, O. (2011) Electrical and Spectroscopic Analysis of Mono- and Multi-Tip Pulsed Corona Discharges in Air at Atmospheric Pressure. *Plasma Sources Science and Technology*, **20**, Article ID: 065002. https://doi.org/10.1088/0963-0252/20/6/065002

[15] Abahazem, A., Merbahi, N., Ducasse, O., Eichwald, O. and Yousfi, M. (2008) Primary and Secondary Streamer Dynamics in Pulsed Positive Corona Discharges. *IEEE Transactions on Plasma Science*, **36**, 924-925. https://doi.org/10.1109/TPS.2008.925708

[16] Ono, R. and Oda, T. (2003) Formation and Structure of Primary and Secondary Streamers in Positive Pulsed Corona Discharge—Effect of Oxygen Concentration and Applied Voltage. *Journal of Physics D*: *Applied Physics*, **36**, 1952-1958. https://doi.org/10.1088/0022-3727/36/16/306

[17] Tarasenko, V.F., Baksht, E.K., Sosnin, E.A., Burachenko, A.G., Panarin, V.A. and Skakun, V.S. (2018) Characteristics of a Pulse-Periodic Corona Discharge in Atmospheric Air. *Plasma Physics Reports*, **44**, 520-532.

https://doi.org/10.1134/S1063780X18050100

[18] Li, Z., Zhang, B. and He, J. (2013) Specific Characteristics of Negative Corona Currents Generated in Short Point-Plane Gap. *Physics of Plasmas*, **20**, Article ID: 093507. https://doi.org/10.1063/1.4823712

[19] Li, Z., Zhang, B., He, J. and Xu, Y. (2014) Influence of Gap Spacing on the Characteristics of Trichel Pulse Generated in Point-to-Plane Discharge Gaps. *Physics of Plasmas*, **21**, Article ID: 012113. https://doi.org/10.1063/1.4863506

[20] Yin, H., Zhang, B., He, J. and Wang, W. (2014) Measurement of Positive Direct Current Corona Pulse in Coaxial Wire-Cylinder Gap. *Physics of Plasmas*, **21**, Article ID: 032116. https://doi.org/10.1063/1.4868966

[21] Liu, Y., Cui, X., Lu, T., Wang, Z., Li, X., Xiang, Y., *et al*. (2014) Detailed Characteristics of Intermittent Current Pulses Due to Positive Corona. *Physics of Plasmas*, **21**, Article ID: 082108. https://doi.org/10.1063/1.4892348

[22] Xu, P., Zhang, B., Chen, S. and He, J. (2016) Influence of Humidity on the Characteristics of Positive Corona Discharge in Air. *Physics of Plasmas*, **23**, Article ID: 063511. https://doi.org/10.1063/1.4953890

[23] Yawootti, A., Intra, P., Tippayawong, N. and Rattanadecho, P. (2015) An Experimental Study of Relative Humidity and Air Flow Effects on Positive and Negative Corona Discharges in a Corona-Needle Charger. *Journal of Electrostatics*, **77**, 116-122. https://doi.org/10.1016/j.elstat.2015.07.011

[24] Britun, N., Gaillard, M., Ricard, A., Kim, Y.M., Kim, K.S. and Han, J.G. (2007) Determination of the Vibrational, Rotational and Electron Temperatures in N2 and Ar-N2 rf Discharge. *Journal of Physics D*: *Applied Physics*, **40**, 1022-1029. https://doi.org/10.1088/0022-3727/40/4/016

[25] Luque, J. and Crosley, D.R. (1999) LIFBASE: Database and Spectral Simulation Program. SRI International Report MP 99-009.

[26] Laux, C.O. (2002) Radiation and Non-Equilibrium Collisional-Radiative Models. Physico-Chemical Modeling of High Enthalpy and Plasma Flows. von Karman Institute Lecture Series 2002-07, von Karman Institute, Rhode-Saint-Gense. http://www.specair-radiation.net

[27] Dubois, D., Merbahi, N., Eichwald, O., Yousfi, M. and Benhenni, M. (2007) Electrical Analysis of Positive Corona Discharge in Air and N_2, O_2, and CO_2 Mixtures. *Journal of Applied Physics*, **101**, Article ID: 053304. https://doi.org/10.1063/1.2464191

[28] Abahazem, A., Guedah, H., Merbahi, N., Yousfi, M., Eichwald, O. and Ihlal, A. (2015) Energy Injected in Multi-Tip Pulsed Corona Discharge Reactor in Air at Atmospheric Pressure for Pollution Control. *Materials Today*: *Proceedings*, **2**, 4694-4700. https://doi.org/10.1016/j.matpr.2015.10.001

[29] Zhu, J., Ehn, A., Gao, J., Kong, C., Aldén, M., Salewski, M., *et al*. (2017) Translational, Rotational, Vibrational and Electron Temperatures of a Gliding Arc Discharge. *Optics Express*, **25**, 3343-3351. https://doi.org/10.1364/OE.25.020243

[30] Wattieaux, G., Yousfi, M. and Merbahi, N. (2013) Optical Emission Spectroscopy for Quantification of Ultraviolet Radiations and Biocide Active Species in Microwave Argon Plasma Jet at Atmospheric Pressure. *Spectrochimica Acta—Part B Atomic Spectroscopy*, **89**, 66-76. https://doi.org/10.1016/j.sab.2013.08.010

[31] Roy, N.C., Hafez, M.G. and Talukder, M.R. (2016) Characterization of Atmospheric Pressure H_2O/O_2 Gliding Arc Plasma for the Production of OH and O Radicals. *Physics of Plasmas*, **23**, Article ID: 083502. https://doi.org/10.1063/1.4960027

[32] Laux, C.O., Spence, T.G., Kruger, C.H. and Zare, R.N. (2003) Optical Diagnostics of Atmospheric Pressure Air Plasmas. *Plasma Sources Science and Technology*, **12**, 125-138.

[33] Bruggeman, P., Iza, F., Guns, P., Lauwers, D., Kong, M.G., Gonzalvo, Y.A., *et al*. (2010) Electronic Quenching of OH(A) by Water in Atmospheric Pressure Plasmas and Its Influence on the Gas Temperature Determination by OH(A-X) Emission. *Plasma Sources Science and Technology*, **19**, Article ID: 015016. https://doi.org/10.1088/0963-0252/19/1/015016

[34] Choi, J.H., Lee, T., Han, I., Baik, H.K., Song, K.M., Lim, Y.S., *et al*. (2006) Investigation of the Transition between Glow and Streamer Discharges in Atmospheric Air. *Plasma Sources Science and Technology*, **15**, 416-420. https://doi.org/10.1088/0963-0252/15/3/017

[35] Obrusník, A., Bílek, P., Hoder, T. and Šimek, M., Z.B. (2018) Electric Field Determination in Air Plasmas from Intensity Ratio of Nitrogen Spectral Bands: I. Sensitivity Analysis and Uncertainty Quantification for Dominant Processes. *Plasma Sources Science and Technology*, **27**, Article ID: 085013. https://doi.org/10.1088/1361-6595/aad663

[36] Zhu, X.M. and Pu, Y.K. (2010) Optical Emission Spectroscopy in Low-Temperature Plasmas Containing Argon and Nitrogen: Determination of the Electron Temperature and Density by the Line-Ratio Method. *Journal of Physics D*: *Applied Physics*, **43**, 24. https://doi.org/10.1088/0022-3727/43/40/403001

[37] Zerrouki, A., Motomura, H., Ikeda, Y., Jinno, M. and Yousfi, M. (2016) Optical Emission Spectroscopy Characterizations of Micro-Air Plasma Used for Simulation of Cell Membrane Poration. *Plasma Physics and Controlled Fusion*, **58**, Article ID: 075006. https://doi.org/10.1088/0741-3335/58/7/075006

[38] Yousfi, M. and Benabdessadok, M.D. (1996) Boltzmann Equation Analysis of Electronmolecule Collision Cross Sections in Water Vapor and Ammonia. *Journal of Applied Physics*, **80**, 6619-6630. https://doi.org/10.1063/1.363785

[39] Itikawa, Y. (2006) Cross Sections for Electron Collisions with Nitrogen Molecules. *Journal of Physical and Chemical Reference Data*, **35**, 31-53. https://doi.org/10.1063/1.1937426